Seismic behaviour of two-dimensional frames made of GFRP pultruded profiles

Pedro Robles Machado Simões Ventura

Department of Civil Engineering, Architecture and Georesources, Instituto Superior Técnico, Universidade de Lisboa, Portugal

Abstract: This paper presents an experimental and numerical study that aimed at evaluating the monotonic and cyclic behaviour of two-dimensional single-storey plane frames made of pultruded GFRP profiles. Two beam-to-column bolted connection systems were analyzed: non-reinforced – comprising two stainless steel cleats; and reinforced – with 8 stainless steel threaded rods connecting the stainless steel cleats to the column's back flange. The reinforcement of the connection aimed at promoting ductility at the beam-to-column connections' level, limiting the damage in the GFRP material. Two monotonic tests were performed per frame type, in order to evaluate their strength, stiffness, failure modes and ductility. Later, a cyclic test was performed per frame type, in order to evaluate their cyclic response, determining their energy dissipation capability. The experiments were simulated with finite element models with a relatively low modelling complexity, using the SAP2000 software. Such models presented a satisfactory agreement with the experimental results, particularly for the initial stages of the response. Both analyses, experimental and numerical, showed that the reinforced connection system has a remarkable effect on the frames' structural behavior, providing significant improvements in terms of their strength and ductility. Nevertheless, the improvements observed in the frames' energy dissipation capability were not significant, and it was found that the introduction of face-to-face bolts had a low influence on the frame's overall stiffness.

Keywords: Beam-to-column bolted connections; Plane frames; Monotonic/cyclic behaviour; Experimental tests; Numerical analysis; Stainless steel.

1. Introduction

Fibre Reinforced Polymers (FRPs) have been gradually gaining acceptance in the field of civil engineering structural applications. The impregnation of fibre reinforcements in a polymeric matrix confer them several advantages over traditional materials (*e.g.*, reinforced concrete and steel), in terms of cost-efficiency and low maintenance over their service life, owing to their non-corrodibility.

Glass Fibre Reinforced Polymer (GFRP) profiles are the most used typology of FRP structural materials in the construction industry, largely due to their reduced cost, high strength-to-weight ratio and durability. Pultrusion manufacturing allows to produce continuously any type of profiles with constant cross-section. The most common cross-sections tend to mimic steel construction, generally exhibiting thin-wall sections [1]. These products have the majority of their fibres oriented in the pultrusion direction, which leads to their orthotropic behaviour, with significant lower stiffness and strength along the transverse directions.

The widespread acceptance of GFRP construction has been hindered by the lack of specific international design standards and limited guidance for their design (especially in seismic areas). The main drawbacks of these profiles, which make the design of pultruded GFRP frames more challenging than traditional structures, lie in their brittle failure, susceptibility to instability phenomena and high deformability [2].

The present work, developed in the frame of the *FRP Quake* project, was driven by the need to understand the sway behaviour of two-dimensional frames made of pultruded GFRP profiles. This study is fundamental to allow a generalized acceptance of these materials. Therefore, monotonic and cyclic full-scale GFRP plane frame tests were performed on two different types of frames. The frames were studied regarding their strength, stiffness and energy dissipation capability. At the same time, a numerical study was conducted, in order to evaluate the feasibility of modelling the frames' behaviour using relatively simple finite element (FE) models.

2. Literature review

The previous studies of structural frames comprising GFRP profiles are few and have seldom involved experimental research. Bank and Mosallam [3,4] performed both creep and short-term static tests on full-scale GFRP plane frames under vertical loads. They

concluded that the main conditioning factors for the frames' design were the strength and the rotational stiffness of the (all-FRP) bolted connections. The premature failure of the structures was associated to the reduced strength of that connection system.

Turvey [5] performed the first load sway tests on a full-scale GFRP frame comprising H-shaped profiles and pultruded web cleated connections (with two GFRP seated angles on the beam's web). The frame exhibited a very flexible structural behaviour, with high sway deflections at the top of the columns and high joint rotations at the maximum applied load (2 kN). Therefore, the author confirmed that the stiffness (deformability) of the connection system is a key parameter of these structures' behaviour.

Na [6] confirmed experimentally and numerically that the beam-to-column connection system (all-GFRP and steel flange cleats) and the bracing scheme are two fundamental parameters in the monotonic sway response of two-stories GFRP frames. With the frames' tests, he achieved significant improvements in strength and stiffness by using steel cleat connections and a diagonal bracing member in each storey. Regarding the numerical analysis, the author calibrated the stiffness of the beam-to-column connections to match the linear stage of the experimental results, concluding that, in general, the connections presented a semi-rigid response.

Minghini and Turkalj [7, 8] presented a numerical buckling analysis about the influence of the warping restraints and the shear deformation effects of the pultruded elements, in the monotonic response of various GFRP plane frames. The frame models comprised thin-walled beam elements with open section, subjected to in-plane lateral loads. The authors showed that, accounting for the non-restrained warping at the column-base connections and the shear deformation effects, the models' performance was strongly affected, leading to a reduced strength and a significant reduced critical buckling load.

Additionally, Minghini *et al*. [7] highlighted the influence of the out-of-plane constraints on the frames' behaviour. They concluded that restraining the models' out-of-plane displacements led to an increased critical buckling load (50-75 %).

Later on, Xiao *et al*. [9] developed a numerical comparative study on the energy dissipation of a GFRP plane frame comprising bonded sleeve connections and steel frames comprising bolted end-plate connections. Although the authors determined experimentally the moment-rotation behaviour of the bonded sleeve connection, in order to develop an accurate joint model for the GFRP frame, they did not perform any experimental investigation on the full-scale frames to validate the numerical results. The pultruded frame's model presented a satisfactory cyclic performance when compared to steel frames, namely regarding energy dissipation capacity. In spite of the GFRP members' lack of ductility, the energy dissipation capacity of this structure was induced by the yielding of steel end-plate from the connection system considered. Therefore, the authors concluded that the ductility of the connection system was a key parameter on the GFRP frames' design, in terms of their energy dissipation capacity, especially in seismic areas.

More recently, the first and only experimental study regarding the sway behaviour of full-scale GFRP plane frames comprising tubular profiles under cyclic loading, was conducted by Martins *et al*. [9, 10]. The authors analyzed the frames' structural behaviour and the influence of infills walls (Figure 1). Higher strength and stiffness, as well as higher cyclic performance, namely regarding energy dissipation, were achieved with infill walls, materialized by composite sandwich panels. Nonetheless, such improvement involved extensive damage in the GFRP elements, undermining their structural integrity.

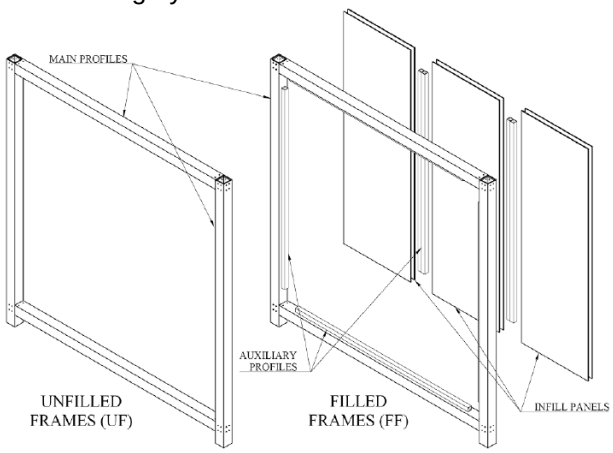

Figure 1 – Overview of the unfilled and filled frames from [11].

Additionally, Martins *et al*. [10, 11] presented a numerical study of the unfilled frames' tests. Although linear-elastic material behaviour was assumed (together with a non-linear experimentally-based constitutive model of the connections), the numerical models provided a fairly good agreement with the experimental data, providing an effective (and conservative) tool for simulation of the cyclic behaviour of pultruded frames. The authors pointed out the feasibility of using simple model in the seismic design of this type of structures.

3. Experimental programme

3.1. Test series

The experimental campaign was performed in the *Laboratório de Estruturas e Resistência dos Materiais* (LERM) of *Instituto Superior Técnico* (IST). The present study consisted of testing two different GFRP plane frame series (non-reinforced and reinforced). Monotonic and cyclic tests were performed aiming at comparing and evaluating the structural performance of these frames.

Four monotonic tests were performed (2 for non-reinforced specimens – series F-NR-M; and 2 for

reinforced specimens – series F-R-M), in order to determine the strength, stiffness and ductility of the frames. For series F-NR-M, only one of the two tests was analyzed, because the first one presented premature failure due to global lateral-torsional buckling of the columns, as discussed in Section 4. Two cyclic tests were performed (1 for a non-reinforced specimen – series F-NR-C and; 1 for a reinforced specimen – series F-R-C), aiming at evaluating the evolution of their strength, stiffness and energy dissipation capability in each cycle. Furthermore, for both experimental analysis, the failure mode in the GFRP elements was assessed.

3.2. Description of the frame components

The experimental sway tests were performed in single-storey closed frames, comprising four pultruded I-shaped profiles (150×75×8 mm^2), made of E-glass fibres and a polyester resin matrix, produced by *ALTO, Perfis Pultrudidos, Lda*. The columns were 3000 mm high and the beams were 2500 mm long, as illustrated in Figure 2.

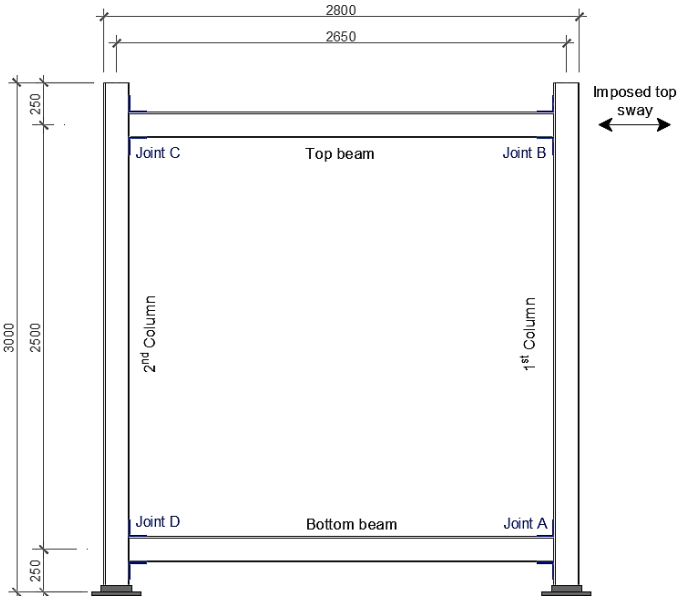

Figure 2 – Geometry of the full-scale frame specimens. Dimensions in mm.

Table 1 presents the main mechanical properties of the GFRP profiles, namely their compressive strengths and elastic modulo in both longitudinal ($\sigma_{cu,L}$ and E_L) and transverse ($\sigma_{cu,T}$ and E_T) directions; distortion modulo (G_{LT}); and Poisson ratio (ν), characterized in a previous experimental campaign performed by Mendes [12].

Table 1 - Main mechanical properties of the GFRP profiles, adapted form Mendes [12].

Property	Average value	Standard deviation
$\sigma_{cu,L}$ (MPa)	328	12,5 %
$\sigma_{cu,T}$ (MPa)	42,3	19,1 %
E_T (GPa)	3,9	29,1 %
E_L (GPa)	41,3	8,7 %
ν (-)	0,29	13,3 %
G_{LT} (GPa)	3,12	15,2 %

The beam-to-column connection systems of the tested frames, developed and studied within the doctoral program of Eng. David Martins (still in development), comprised two stainless steel (AISI 304) flange cleats and 4 stainless steel bolts M8 (A2-70) per flange, as illustrated in Figure 3 a) – c). Additionally, 8 stainless steel threaded rods connecting the steel cleats to the column's flanges were used at each reinforced connection. Four monotonic tests were performed (2 for non-reinforced frames – series F-NR-M; 2 for reinforced frames – series F-R-M).

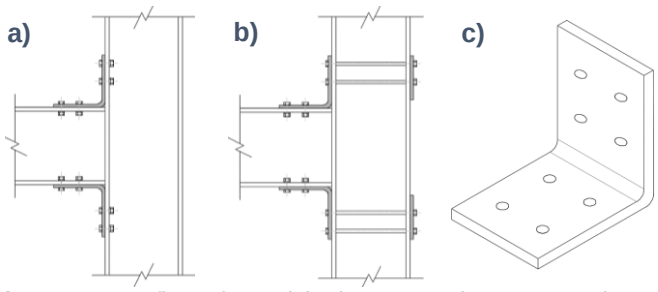

Figure 3 – Configurations of the beam-to-column connections: **(a)** non-reinforced; **(b)** reinforced, developed by Eng. David Martins. **(c)** 3D view of steel cleats used.

The web-crippling phenomenon observed in the 2nd column's pultruded profile (at joint C), for the first monotonic test (F-NR-M1), further discussed in Section 4, led to an experimental study intended to develop and evaluate a web reinforcement system. Nine experimental web-crippling tests (Figure 4 a) were performed, using the end two flanges (ETF) configuration, studied by Fernandes [13]. Three specimens were analyzed: non-reinforced (ETF-NR series); and reinforced with two stainless steel cold-formed plates with 2 and 4 mm of thickness, on each face of the specimen's web (ETF-R2 and ETF-R4 series).

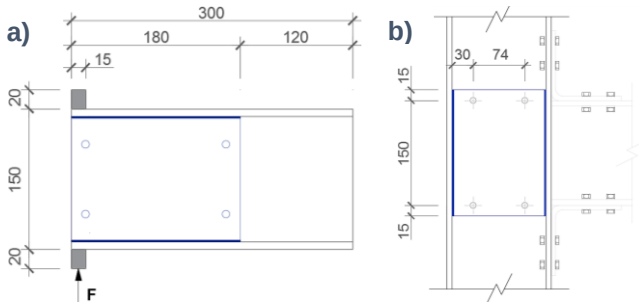

Figure 4 – **(a)** Web-crippling tests' configuration. **(b)** Detail of web reinforced column. Dimensions in mm.

Regarding the web-crippling experimental results, specimens of series ETF-R4 showed the best mechanic performance, with increases of 84% and 133% of the stiffness and resistance, respectively, comparing to the non-reinforced series. Thus, the columns' webs were reinforced at all frames' joints with two stainless steel cold-formed plates with 4 mm thickness, bolted to each other, as illustrated in Figure 4 b).

3.3. Test setup

Both monotonic and cyclic tests were performed in a reaction wall. The displacements were imposed at the frames' top beam by a hydraulic jack, with capacity of 1000 kN and stroke of ± 200 mm, mounted in the reaction wall. In the cyclic tests, two *dywidag* bars were used together with the hydraulic jack in order to allow the reversing of the loading direction in the setup plan.

The frames' bases were clamped to a cylindrical steel piece (with 4,5 cm deep grooves) bolted to a thick steel plate, the latter being bolted to a rigid beam anchored to laboratory's strong floor. At the end of F-NR-M1 test significant vertical displacements on the 1st column's base were observed. Therefore, two stainless steel cleats were placed in each face of the column web, and bolted to the pultruded profile and to the cylindrical steel piece (Figure 5), reducing the displacements and rotations at the frames' bases. Nonetheless, on the F-NR-M2 test, the columns' bases presented extensive shear-out damages due to significant displacements and rotations, as discussed in Section 4. Therefore, an all-steel restraining system comprising 4 UPN100 profiles, 4 threaded rods and 4 bars, depicted in the left bottom corner of Figure 5, was also added in order to reduce the shear forces on the steel bolts.

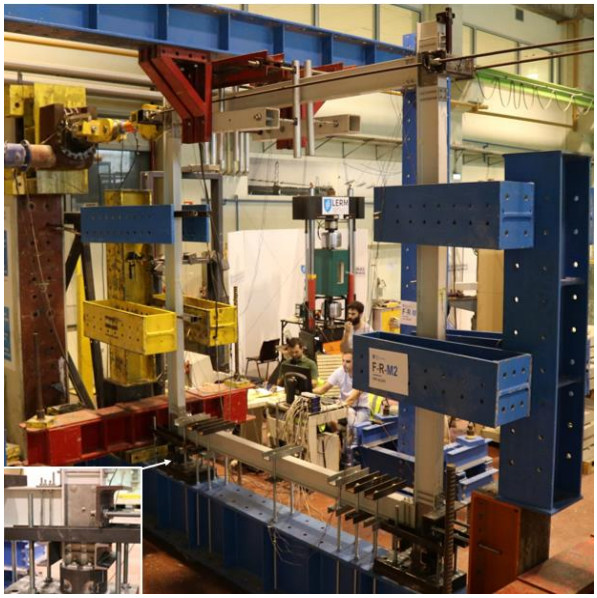

Figure 5 - Test setup for: F-R-M2, F-NR-C1 and F-R-C1 tests.

Additionally, in order to restrict the vertical displacements of the bottom beam, 7 vertical restraining fixtures were used, as illustrated in Figure 5, comprising two UPN100 steel profiles and two stainless steel bars fixed to the rigid beam. The bottom beam's horizontal displacements were prevented by 1 (or 2 in case of cyclic tests) steel plate(s) oriented vertically and centered with the beam's longitudinal axe (Figure 5).

The out-of-plane displacements of the top beam were prevented by four aluminum bars fixed to a steel frame anchored to the laboratory's strong floor. Concerning the out-of-plane displacements of the columns, no additional bracing system was applied in the F-NR-M1 test. This frame presented significant out-of-plane displacements, leading to global lateral-torsional buckling of the columns of the frame, as discussed in Section 4. Thus, this failure mode was prevented by applying a lateral bracing system on both columns, placed at a vertical distance of ~1,8 m from the top flange of the bottom beam. Nonetheless, the lateral-torsional buckling of the columns, namely of the 2nd column, was observed at F-R-M1 test, due to higher in plane displacements applied on reinforced frames. For the remaining tests, two lateral bracing systems were applied in both columns, placed at vertical distances of ~0,8 m and ~1,6 m from the top flange of the bottom beam (Figure 5), in order to avoid buckling phenomena.

3.4. Instrumentation and load protocol

Figure 6 illustrates the position of the instrumentation used, namely: (i) F, the load cell (capacity of 300 kN); (ii) S_i, the string pot displacements transductors (stroke of 500 mm); (iii) D_i, the displacement transducers (strokes ranging from 10 mm to 100 mm), for measuring the midspan displacements (D_{1-2}) and the rotations at the bottom connection (D_{3-4} and D_{5-6}, in the 1st column and bottom beam, respectively). (iv) I_i, the inclinometers (measuring range of ±10º); and (v) e_i, the electrical strain gauges, applied in 9 sections of the frames F-NR-M2 and F-R-M2. All the parameters were sampled at a rate of 10 Hz by two data loggers.

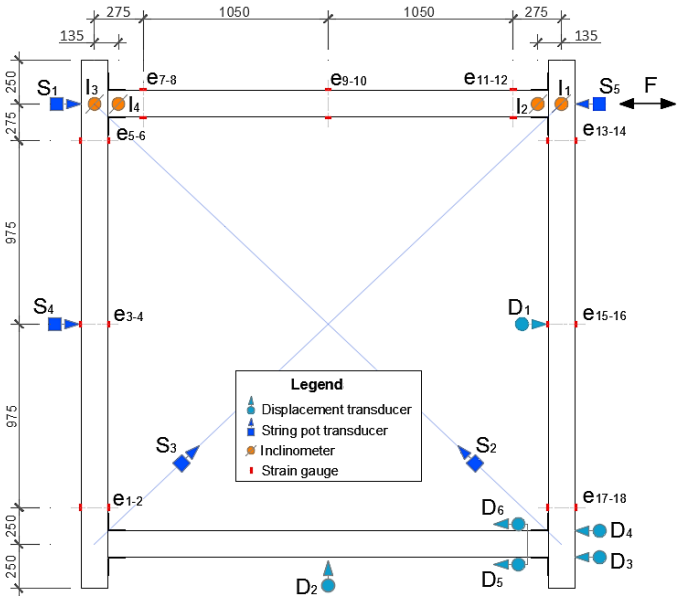

Figure 6 – Instrumentation scheme of the test specimens. Dimensions in mm.

The monotonic tests were carried out under displacement control at an average speed of 30 mm/min until either the brink of the specimen's collapse, by evident damage/buckling, or the hydraulic jack's maximum stroke was reached.

The cyclic tests followed the recommendations of ECCS [14], regarding the definition of the displacement

history. The definition of the cycles was based on the "yield" displacements (D_{el}) determined from the monotonic tests, which characterize the limit of the frames' elastic response. Thus, only one displacement history was defined ($D_{el,av}$ = 17 mm for both typologies). Nine cycles were defined, as illustrated at Figure 7.

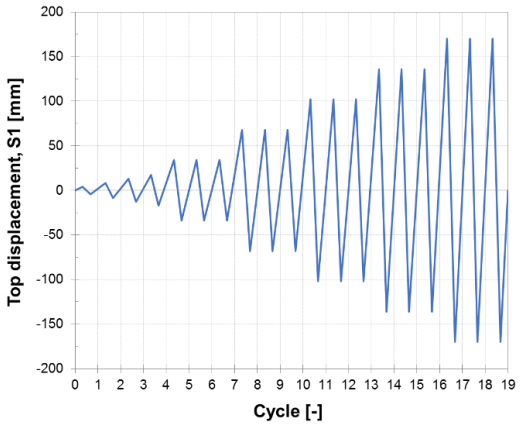

Figure 7 – Loading history protocol of the cyclic tests.

4. Experimental results and discussion

4.1. Monotonic tests

As mentioned, two monotonic tests were performed per series, in order to determine their strength and stiffness, as well as to determine their failure modes. It is worth mentioning that the first test, F-NR-M1, was not considered valid and, therefore, those results are not included in the present document, due to the premature lateral-torsional buckling failure. This damage was observed when the top displacement was around 93 mm.

The monotonic load *vs.* top displacement (S_1)/ top drift (Φ) experimental curves are illustrated at Figure 8.

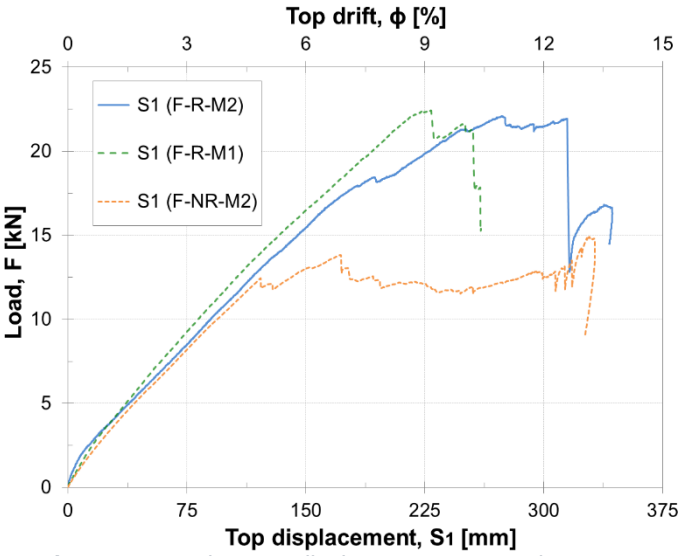

Figure 8 – Load *vs.* top displacement monotonic curves.

All frames seemed to exhibit an initial very stiff linear behaviour for top displacements ranging from 12 to 21 mm, until a stiffness reduction was observed. This reduction may be associated to minor initial adjustments, given that no visual damage or audible crack noises were identified. Afterwards, all the tested frames presented a second approximately linear stage until the occurrence of the first local damage. The first damage observed was common to all specimens, comprising the development of shear-out cracks in the bolted connection system of both GFRP column bases. This damage, illustrated in Figure 9 a), progressed throughout the tests, during which the width of those cracks increased significantly.

The non-reinforced frame under monotonic load (F-NR-M2) after the first damage (S_1 = 120 mm, F = 12,4 kN) started to exhibit non-linear behavior with successive peak loads, consequence of several local failures. Afterwards, web-crippling due to transverse compression stresses and web-flange junction tensile rupture occurred at the bottom beam near joint D (Figure 9 b). After those damages the load *vs.* displacement curve exhibited an approximately horizontal stage until the maximum load was reached ($F_{máx}$ = 14,9 kN). The end of this test was caused by loss of structural integrity, due to shear-out rupture of the 1st column base (*cf.* Figure 9 a).

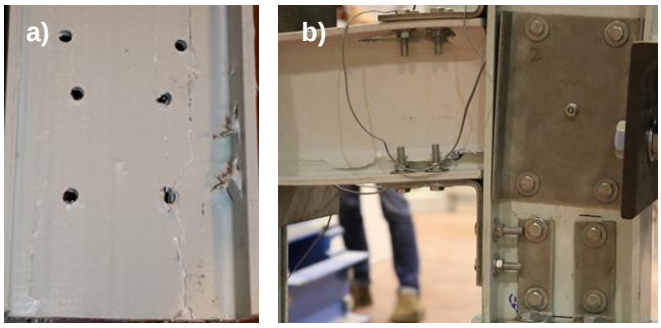

Figure 9 – **(a)** Shear-out at the column base of F-R-M1 frame. **(b)** *Web-crippling and web-flange junction tensile rupture at bottom beam (joint D) of F-NR-M2 frame.*

Both reinforced frames (F-R-M1 and F-R-M2) presented identical strength and stiffnesses values. Nonetheless, after the columns bases' shear-out rupture, the failure modes observed were very distinct. For the frame F-R-M1 this failure was reached for the maximum load applied ($F_{máx}$ = 22,5 kN). Afterwards, a sudden reduction of the load was observed, followed by a short load increase until the interruption of the test due to the crushing of the web-flange junction in compression of 2nd column. As observed for F-NR-M1 frame and as mentioned before, this failure and therefore the strength of the F-R-M1 frame was limited by the lateral-torsional buckling phenomenon, as illustrated in Figure 10 a).

For the frame F-R-M2, the shear-out rupture occurred for an imposed load of 18,5 kN. Afterwards, the frame exhibited a gradual decrease of stiffness until the maximum load was reached ($F_{máx}$ = 22,1 kN). This reduction of stiffness was associated with the progression of the crushing damage at the (top) web-flange junction of the top beam, near joint C. After that, a short horizontal stage was observed in the load vs. displacement response until a sudden load reduction was registered, for a top displacement of 315 mm. The end of the test was limited by the crushing of the 2nd column's web near the steel plate of the horizontal restraining system (Figure 10

b), due to the compressive stresses induced by the bottom beam and due to the extremely large column's drift at this stage of the test. This damage was followed by the occurrence of severe damage, with failure concentrating mainly at the columns.

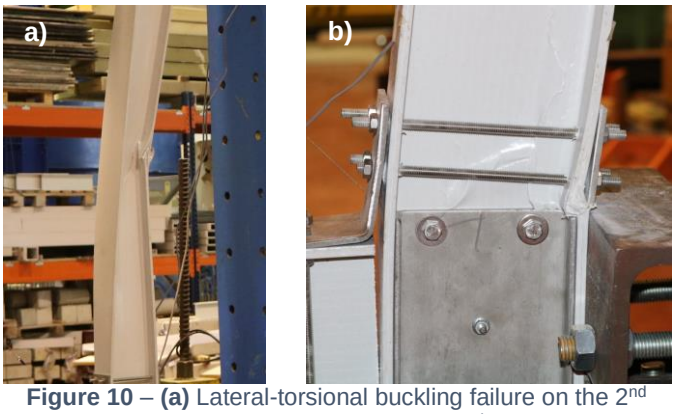

Figure 10 – **(a)** Lateral-torsional buckling failure on the 2nd column of F-R-M1 frame. **(b)** Crushing of 2nd column's web in compression, of the F-R-M2 frame (joint D).

Regarding the rotations measured at the top (joints B and C) and bottom (joint A) joints, it is worth noting that, in general, the rotations measured at the columns were much higher than those measured at the beams. Therefore, the rotations of the beams were considered negligible, due to the higher flexural deformation exhibited by the columns. Additionally, as expected, the absolute relative rotations at the top joints were higher than those determined for the bottom joint, owing to the higher rotational restraint on the vicinity of the column bases.

Table 2 summarizes the main results of the monotonic tests, namely the initial and secondary stiffness (K_1 and K_2), the load (F), the top displacement (S_1), top drift (Φ) and the relative rotation measured at joint B (ΔI_{1-2}), corresponding to the elastic limit and to failure.

As mentioned, the bending moments were calculated from the strain measurements, considering material linear (elastic) behaviour, constant curvature of the beams' cross-section and linear distribution of bending moments (M= (EI).1/R). Figure 11 and 12 illustrate the bending moment distributions in the members of frames F-NR-M2 and F-R-M2, respectively. Two different load levels were studied: (i) the elastic limit load (2,4 kN and 2,3 kN for the frames F-NR-M2 and F-R-M2, respectively); and (ii) the maximum admissible load considering the assumptions of the beam's model used, namely regarding the linearity of the bending moment distribution (9,4 kN and 11,0 kN for the frames F-NR-M2 and F-R-M2, respectively).

As expected, for the load range analyzed, the bending moment distribution of both frames was very similar and consistent with a linear distribution. The columns' presented a symmetrical bending moment distribution, with higher bending moments in their bases, where the GFRP profiles were connected to the rigid support, due to the higher rotational restrain degree.

It should be mentioned that for both specimens, while the beams exhibited a point with approximately null bending moment at mid-span throughout all test, in the

Table 2 – Main results of the monotonic GFRP frame tests.

Limit	Test	F [kN]	Φ [%]	K_1 [kN/m]	K_2 [kN/m]	S_1 [mm]	ΔI_{1-2} [°]
Elastic limit	F-NR-M2	2,4	0,7	138	97	18	0,35
	F-R-M1	3,2	0,9	160	100	21	0,29
	F-R-M2	2,3	0,5	182	95	12	0,24
Maximum load	F-NR-M2	14,9	13,6	-	-	329	6,20
	F-R-M1	22,5	9,4			229	4,78
	F-R-M2	22,1	11,3			274	5,45

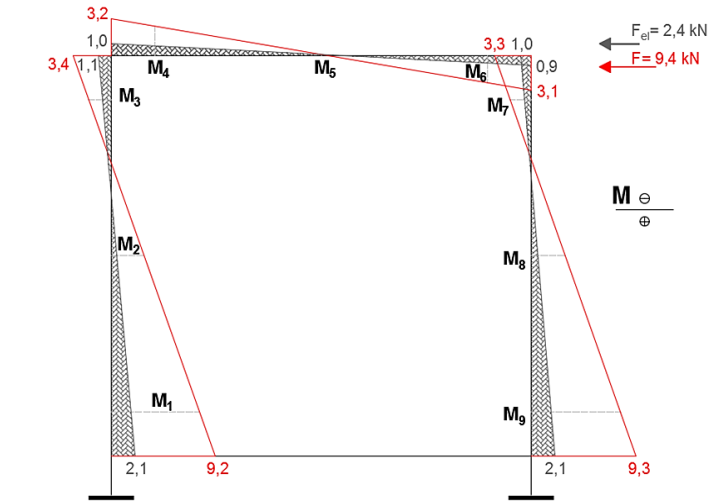

Figure 11 – Bending moment distribution in the F-NR-M2 test. Bending moments in kN.m.

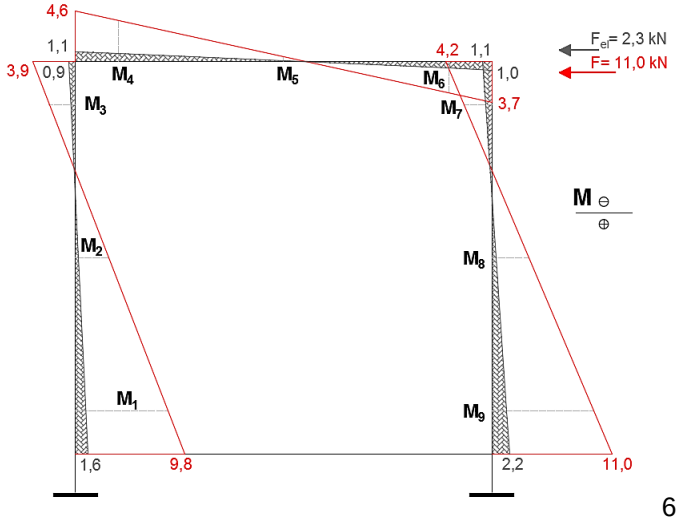

Figure 12 – Bending moment distribution in the F-R-M2 test. Bending moments in kN.m.

columns this point progressed to the top of the columns, as the imposed top displacement increased. These results show that as the tests progressed, the joints accumulated damage (and non-linear strains in the stainless steel) which led to the reduction of their rotational stiffness.

Figure 13 presents the bending moment *vs.* relative rotation ($\Delta\theta = \Delta l_{1\text{-}2}$) curves of joint B of the 1st column, for the frames F-NR-M2 and F-R-M2. The curves for the full-scale connection tests (performed by Eng. David Martins) are also illustrated, both regarding the non-reinforced and reinforced connection systems. For the reinforced system, it was considered the case without (NR) and with (R4) two stainless steel plates with 4 mm of thickness reinforcing the columns' web.

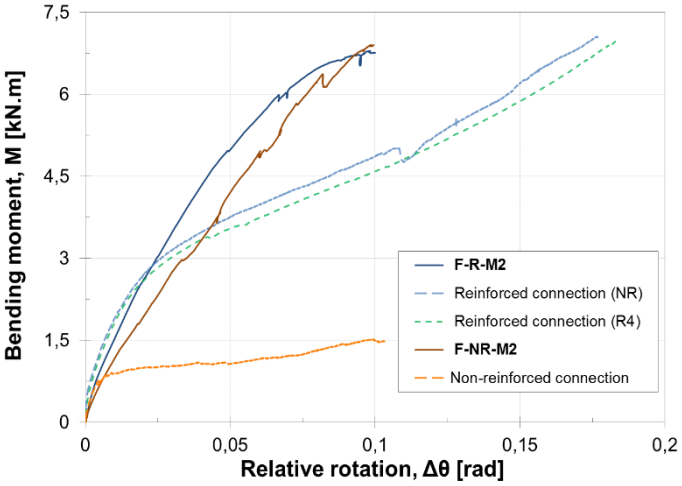

Figure 13 – Moment vs. relative rotation curves of joint B of: frames F-R-M2 and F-NR-M2; and full-scale beam-to-column tests of the doctoral program of Eng. David Martins.

The frames F-NR-M2 and F-R-M2, after an initial (stiffer) linear stage, characterized by a rotational stiffness ($K_{\theta,1}$) of 181 and 202 kNm/rad, respectively, presented an approximately linear behaviour, with ~46% of the initial rotational stiffness. Nonetheless, the frame F-NR-M2 exhibited almost linear behaviour until the end of the test, while for frame F-R-M2 this proportionality was lost after a relative rotation of ~0,05 rad, followed by a gradual reduction of rotational stiffness. For both specimens, the maximum bending moment was reached at the end of the test, for the same relative rotation value ($\Delta\theta_{M(máx)}$=0,10 rad), attaining very similar values (6,9 and 6,8 kNm for the frames F-NR-M2 and F-R-M2, respectively).

It is worth mentioning that, despite exhibiting an initial stage similar to that verified in the frame connection, the full-scale connection tests diverged from the former for M > Mel (= 0,9 and 0,8 kNm for the frames F-NR-M2 and F-R-M2, respectively). These differences are justified by the fact that the connection tests were performed on a column with both extremities fixed, simulating an intermediate storey connection, whereas joint B presented an upper free-end edge.

Lastly, performing a comparative analyses of the monotonic results presented for both specimens, it is noted that the reinforcing system used in the beam-to – column connections improved significantly the strength of the frame (~50%). This system also avoided the occurrence of premature brittle failure modes at the vicinity of the top connections, namely the tensile rupture of the web-flange junction and the punching shear of the steel bolts. Nonetheless, both series presented very similar elastic properties, regarding stiffnesses and elastic limit load. These results clearly indicate the influence of the stainless steel rods connecting the column's flanges on the mobilization of all column's cross-section, allowing a better stress distribution.

4.2. Cyclic tests

In the analyses of the cyclic test results, apart from the load *vs.* displacement curves and the failure modes, which are presented in the following section (*cf.* Section 5.2), three parameters set by ECCS [14] were considered, namely: (i) strength ratio; (ii) stiffness ratio; and (iii) absorbed energy. These parameters were defined for positive and negative paths (semi-cycles).

Table 3 presents the maximum loads (F) of each cyclic test, and their respective top displacements (S_1), for both loading directions. As expected from their symmetrical geometry, until the final stage of the tests both experimental series (F-NR-C1 and F-R-C1) presented hysteretic curves with symmetric behaviour. Nonetheless, for the final cycles the mechanical properties of the frames in the positive direction were much higher when compared to the negative direction, due to the local damage progression in the first half of the cycles (positive). It should be mentioned that the monotonic response, in general, corresponded to the envelope of the hysteretic curves.

Table 3 – Maximum load points of the cyclic frame tests.

Test	F_{max} [kN]	F_{min} [kN]	$S_{1,max}$ [mm]	$S_{1,min}$ [mm]
F-NR-C1	16,5	-13,1	188	-170
F-R-C1	17,7	-15,7	171	-166

Regarding the main failure modes of the cyclic tests, they were similar to those observed in the monotonic tests. The frame F-NR-C1 presented: (i) web-flange junction tensile damage; (ii) tearing of the mats of the GFRP columns' flange and punching shear of the steel bolts at the top beam-to-column connections; (iii) shear-out rupture in the bolted connection system of both GFRP column bases. The frame F-R-C1 exhibited less premature local damage accumulation, as mentioned, as the stainless steel rods provided a better stress distribution. However, the reinforced frame presented: (i) web-crippling at both top connections; and (ii) top beam's web-flange junction tensile rupture (near joint B).

Figure 14 illustrates the strength ratio evolution per cycle, for both frames. An ascending tendency was observed until the 5th cycle, when the "yield" displacement was exceeded. Afterwards, with the local damage progression, the cycles for the same displacements showed an approximately constant strength ratio. However, when the displacement was increased the strength slightly increased. It is worth mentioning that both frames presented a similar strength ratio evolution throughout the cyclic tests.

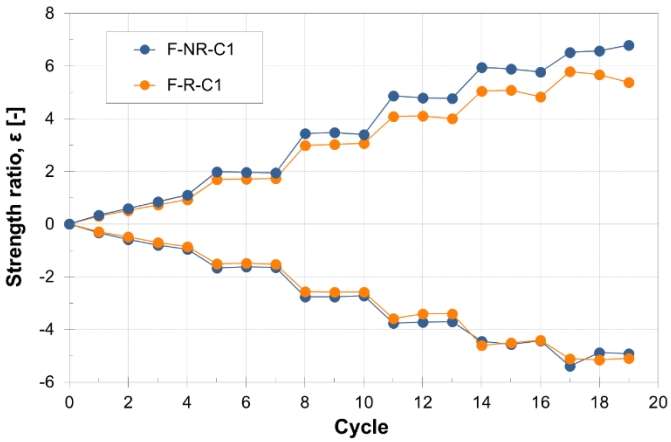

Figure 14 – Strength ratio evolution of the cyclic tests.

Figure 15 presents the stiffness ratio evolution per cycle. Both frames exhibited a decreasing trend throughout the cyclic tests. This shows that, as discussed before, the evolution of the local damage accumulation reduces significantly the frames' stiffness.

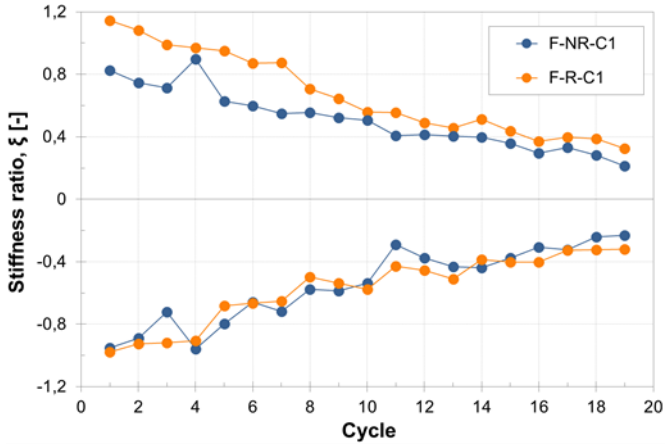

Figure 15 – Stiffness ratio evolution of the cyclic tests.

Figure 16 shows the total absorbed energy per cycle. As expected, until the 10th cycle both frames presented a very similar behaviour. For the subsequent cycles the reinforced frame (F-R-C1) exhibited higher energy values than the F-NR-C1 frame (~18% at the end of the test). It should be mentioned that this difference was not as accentuated as expected. This was justified by the geometry of the studied frames; in fact, the connection in the full-scale connection tests simulated an intermediate storey connection, whereas in the frames they simulated a top storey, and therefore the former connections were more loaded than the latter (frames).

From these results, it was possible to conclude that the face-to-face steel rods of the reinforcing connection system allowed to explore better the ductility of the steel elements, having a great influence on the frames' capacity to absorb energy.

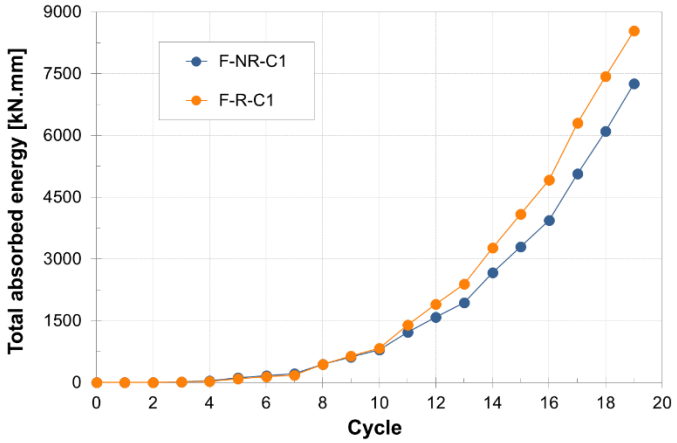

Figure 16 – Total absorbed energy evolution of the cyclic tests.

5. Numerical analysis

5.1. Model description

The numerical analysis presented in this document was developed resorting to the finite element (FE) software SAP2000. Figure 17 illustrates the numerical two-dimensional model used to simulate the cyclic sway tests.

The GFRP material was modelled as orthotropic, considering the mechanical properties determined by Mendes [12], presented in Table 1. It is worth mentioning that, in this numerical analysis, the damage and its progression on the GFRP material was not considered, in order to reduce the numerical effort. The structural profiles were modeled as frame elements, with their real lengths (2,5 m and 3,0 m for beams and columns, respectively) and constant I-shaped cross-section (150×75×8 mm^2).

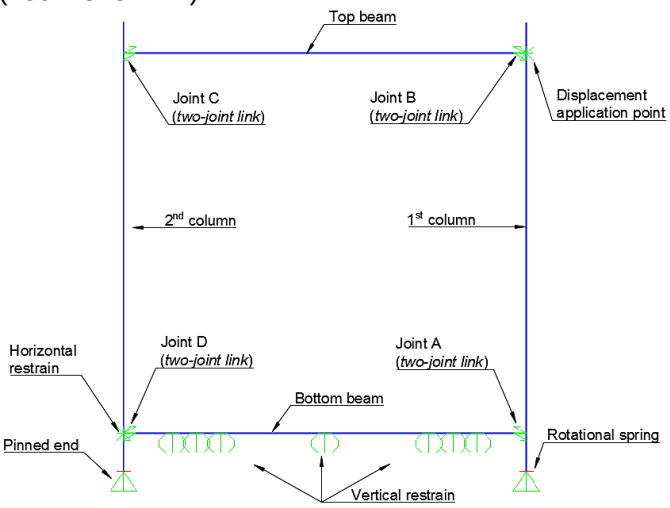

Figure 17 – Numerical model, with boundary conditions and identification of all elements.

The beam-to-column connections were modelled as non-linear 2-joint links, considering all directions fixed

with the exception of the rotations around the out-of-plane orthogonal axis (R3). These rotations were modelled with the experimental moment *vs.* rotation curves of the full-scale connection tests, performed by David Martins, and using the Pivot hysteresis model [15]. The parameters that defined this model were calibrated based on the comparison between numerical moment *vs.* rotation curves from the FE model of the beam-to-column connection and the experimental curves determined from the full-scale tests. It should be mentioned that the parameters were also calibrated on the frames' model regarding their global behaviour. With this analysis, it was concluded that considering symmetrical behaviour (with $\alpha = 100$ and $\beta = 1{,}0$), both connection typologies presented a fairly good agreement between numerical and experimental curves.

The stiffness of the base connections was calibrated based on the numerical and experimental frames' global stiffnesses. Therefore, they were modelled as semi-rigid connections. In this regard, a linear joint spring was adopted for the rotations around the out-of-plane orthogonal axis (R3), with a rotational stiffness of 500 kN/m. Additionally, the horizontal and vertical restraining fixtures used at the bottom beam (*cf.* Figure 5) were simulated by restraining the displacements in the X and Z directions, respectively.

5.2. Results and discussion

In-plane geometrically linear analysis was performed by means of an imposed sway displacement, at the point of the applied load (*cf.* Figure 17). The loading history protocol followed the experimental tests (*cf.* Section 3.4).

Figure 18 presents the monotonic numerical and experimental load *vs.* top displacement curves obtained for both frames (NR – non-reinforced; and R – reinforced).

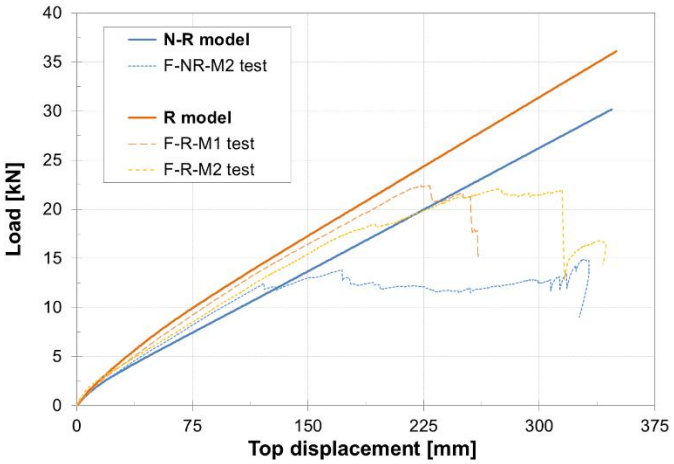

Figure 18 – Experimental and numerical load *vs.* top displacement monotonic curves.

The numerical and experimental curves of the non-reinforced frame presented very similar paths until the elastic limit load was reached. Afterwards, the FE model exhibited ~32% lower stiffness, and this reduction was due to the non-linear behaviour determined in the connection tests. However, the non-reinforced frames' connections showed non-linear behaviour just after the occurrence of the first damage (F = 12,4 kN). For the reinforced frame, an overall reasonable agreement was achieved for the analyzed curves until the first (experimental) damage occurred. This is justified by the assumptions made when developing the models, namely the fact that the damage in the GFRP material was not accounted for in the FE models.

Regarding the domain of application of the FE models, in general, the models presented a very good agreement with the experimental tests, in terms of the frames' global stiffness

Figure 19 and 20 compare the load *vs.* top displacement hysteretic curves determined from the numerical models and those obtained in the experimental tests, for non-reinforced and reinforced frames, respectively.

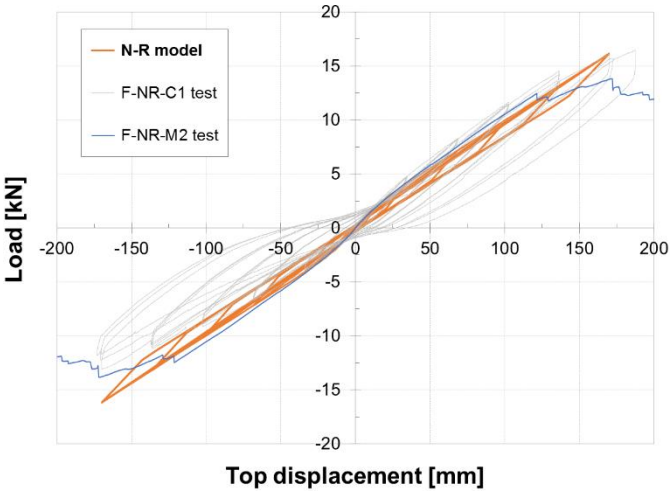

Figure 19 – Experimental and numerical load *vs.* top displacement cyclic curves, for non-reinforced frames.

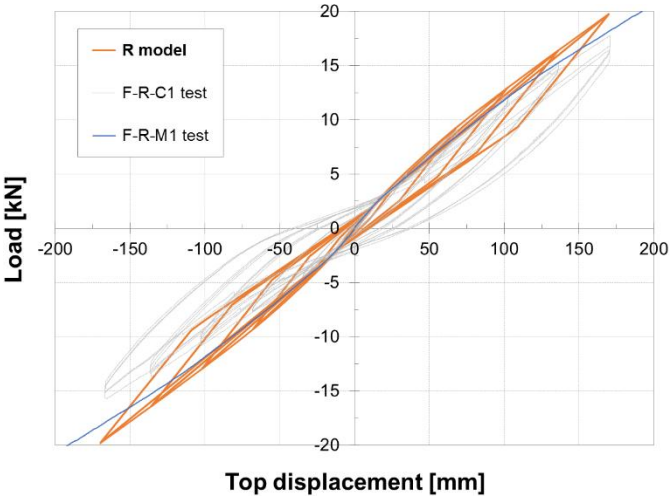

Figure 20 – Experimental and numerical load *vs.* top displacement cyclic curves, for reinforced frames.

The results obtained show that the numerical models presented an overall satisfactory agreement with the experimental tests, especially for the reinforced frame. Nonetheless, for the last cycles of both frames, the experimental hysteretic loops were larger than their numerical counterparts, mainly regarding the unloading paths. As mentioned, these differences are explained by

the fact that damage in the GFRP profiles was not accounted in the numerical models.

In terms of the frames' strength and stiffness evolution, until the 8th and 11th cycles for the F-NR-C1 and F-R-C1 frames, respectively, the FE models presented identical behaviour to the tests. It should be mentioned that these cycles corresponded to the visual observation of significant local damage accumulation during the experimental tests.

Concerning the evolution of the total absorbed energy, Figure 21 compares the experimental and numerical results. It can be seen that, in general, the FE models underestimate the accumulated energy, mainly for the non-reinforced (N-R) model. After 19 cycles, the total absorbed energy determined from the models of the non-reinforced (NR) and reinforced (R) frames were, respectively, -63% and -32% than their experimental counterparts, due to the aforementioned reasons.

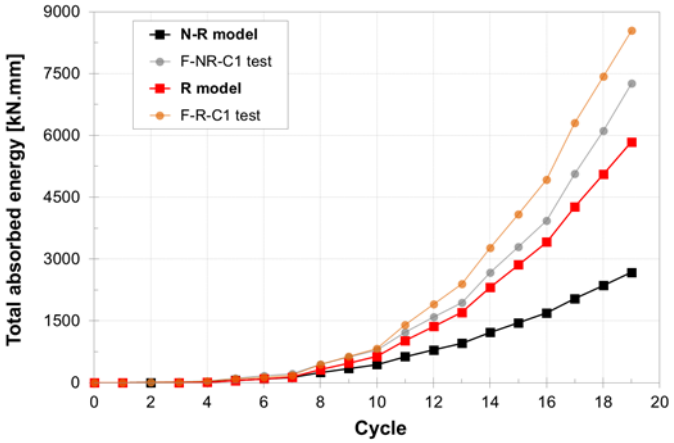

Figure 21 – Total absorbed energy evolution of the cyclic experimental tests and numerical analysis.

6. Conclusions

This paper presented an experimental and numerical study about the lateral sway behaviour of GFRP two-dimensional frames.

The experimental study showed that the reinforced frames provided the best structural performance, being able to resist higher levels of load for significant deformations (~50%). However, similar values of stiffness were observed for both frame types. Therefore, the reinforced frame was chosen to integrate the *FRP Quake* project.

The main drawback of the chosen solution in the scope of the present project is the fact that it exhibited an elastic (linear) behaviour until very high top displacements, which were reflected in modest gains of absorbed energy, when compared to the non-reinforced frame. Therefore, for seismic design purposes, it is accurate (and conservative) to consider that both analysed frame structures present linear behaviour until collapse (brittle rupture).

Lastly, concerning the numerical study, the models developed were fairly able to simulate the monotonic and cyclic response of the analyzed frames. Although the FE models did not simulate the damage in the GFRP material, as it was assumed to present linear and elastic material behaviour, they were still able to provide a relatively good simulation of the frames' experimental response. The aforementioned reasons pointed out the feasibility of considering simple FE models in the design of pultruded frames, especially in seismic areas.

7. References

[1] Correia, J.R. (2015). Fibre-Reinforced Polymer (FRP) Composites. In F. Margarido e M.C. Gonçalves (Eds.), Materials for Construction and Civil Engineering: Science, Processing, and Design, capítulo 11, 501-556, Springer, Dordrecht.

[2] Hizam, R.M., Manalo, A.C., Karunasena, W. (2013). Effect of mechanical insert on the behaviour of pultruded fibre reinforced polymer (FRP) bolted joint. Fourth Asia-Pacific Conference on FRP in Structures (APFIS 2013), Melbourne, Austrália.

[3] Bank, L.C., Mossallam, A.S. (1992). Creep and failure of a full-size fiber-reinforced plastic pultruded frame. Composites Engineering, 2(3), 213-227.

[4] Mosallam, A.S., Bank, L.C. (1992). Short-term behavior of pultruded fiber-reinforced plastic frame. Journal of Structural Engineering, 118(7), 1937-1954.

[5] Turvey, G.J. (1996). Testing of pultruded GRP pinned base rectangular portal frame for the EUROCOMP project. EUROCOMP Design Code and Handbook, 719-741, Londres.

[6] Na, G.S. (2008). Load-Displacement Behavior of Frame Structures Composed of Fiber Reinforced Polymeric Composite. Tese de Doutoramento em Engenharia Civil, School of Civil and Environmental Engineering, Georgia Institute of Technology.

[7] Minghini, F., Tullini, N., Laudiero, F. (2008). Buckling analysis of FRP pultruded frames using locking-free finite elements. Thin-Walled Structures, 46, 223-241.

[8] Turkalj, G., Lanc, D., Banić, D., Banić, J., Vo, T.P. (2018). A shear-deformable beam model for stability analysis of orthotropic composite semi-rigid frames. Composite Structures, 189, 648-660.

[9] Xiao, X., Zhang, Z., Bai, Y. (2017). Comparative study of energy dissipation capacity of steel and glass fibre-reinforced polymer frames with bonded sleeve connections. Journal of Reinforced Plastics and Composites, 36(22), 1665-1679.

[10] Martins, D., Sá, M., Gonilha, J., Correia, J.R., Silvestre, N., Ferreira, J.G. (2019). Experimental and numerical analysis of GFRP frame structures. Part 2: Monotonic and cyclic sway behaviour of

plane frames. Composite Structures, 220, 194-208.

[11] Martins, D., Proença, M., Gonilha, J., Sá, M., Correia, J.R., Silvestre, N. (2019). Experimental and numerical analysis of GFRP frame structures. Part 1: Cyclic behaviour at the connection level. Composite Structures, 220, 304-317.

[12] Mendes, J.D. (2017). "*Comportamento Mecânico de Ligações aparafusadas em Materiais FRP"*. Master Dissertation in Civil Engineering, Instituto Superior Técnico, University of Lisbon.

[13] Fernandes, L. (2014). *Comportamento Estrutural de Vigas de GFRP Submetidas a Forças Concentradas: Caracterização Experimental, Modelação Numérica e Estudo Analítico*. Dissertação de Mestrado Integrado em Engenharia Civil, Instituto Superior Técnico, Universidade de Lisboa.

[14] European Convention for Constructional Steelwork (ECCS). (1986). *Recommended Testing Procedures for Assessing the Behaviour of Structural Steel Elements under Cyclic Loads*, 45, Roterdão, Holanda.

[15] Dowel, R.K, Seible, F., Wilson, E.L. (1998). Pivot Hysteresis Model for Reinforced Concrete Members. American Concrete Institue (ACI) Structural Journal, 95(5), 607-617.